

Application of the Wave Based Prediction Technique for structural problems with stress singularities

C. Vanmaele, D. Vandepitte, W. Desmet

K.U.Leuven, Department of Mechanical Engineering,
Celestijnenlaan 300 B, B-3001, Heverlee, Belgium
e-mail: caroline.vanmaele@mech.kuleuven.be

Abstract

The Finite Element Method is a commonly used prediction method for dynamic simulations of plate bending problems. A major disadvantage of this method is its practical frequency limitation in that the computational loads become prohibitively large at higher frequencies. A newly developed Wave Based prediction technique aims to relax this frequency limitation through an enhanced computational efficiency. This paper discusses the application of the Wave Based Method for the particular case where stress singularities appear in one or more corners of a polygonal plate domain. In this case the conventional set of field variable expansion functions is extended with some special-purpose functions which incorporate the corner point singularities. The beneficial convergence rate of the Wave Based Method as compared with the Finite Element Method is verified for various validation examples.

1 Introduction

In recent years, the vibrational and acoustic behaviour of a product became a criterion of growing importance in the product design process. This behaviour is often determined predominantly by the steady-state dynamic deformations of the mechanical structure. In view of supporting design decisions through virtual prototyping, it is important to have efficient numerical prediction techniques that are capable of making accurate structural predictions.

Deterministic element based techniques, such as the Finite Element Method (FEM) [1], are most commonly used for dynamic simulations of mechanical structures. These methods are based on the discretisation of the structure into small elemental domains. They express the dynamic field variables within each element in terms of local, predefined shape functions, that only satisfy the Dirichlet boundary conditions and that do not fulfil the governing differential equations. The solution is determined by restoring the constitutive relations and Neumann boundary conditions in an integral sense. As a result, the number of elements and the subsequent size of the models increase with increasing frequencies, such that the use of these deterministic methods is practically limited to low-frequency applications.

Statistical prediction techniques form a second class of numerical methods. The SEA method [2] is the prominent technique of this class. This method divides the structure into a number of subsystems, for which only space- and frequency-averaged energy levels are predicted. The SEA method is only applicable if each subsystem meets some conditions such as a high modal overlap, which limits the use of the statistical methods to high-frequency applications. Between the upper frequency limit of the deterministic techniques and the lower limit of the statistical techniques, lies the so-called mid-frequency range, for which no mature and efficient prediction techniques are available.

This paper proposes a Wave Based Method (WBM) that is based on the indirect Trefftz method [3] for the dynamic analysis of plate bending problems. Instead of dividing the problem domain into a large number of elemental domains, the WBM divides the domain into large, convex subdomains. Within each subdomain

the field variables are expressed in terms of global wave function expansions, which exactly satisfy the governing dynamic equations. This implies that there is only an approximation involved in the boundary and interface conditions. Consequently the system matrices are substantially smaller as compared with the FEM. The smaller system matrices result in an enhanced computational efficiency, which allow the WBM to become also applicable in the mid-frequency region.

In many plate bending problems stress singularities arise in the problem solution. For a polygonal plate domain, the bending stresses often become singular in the corners. In general, it is difficult to achieve accurate prediction results whenever singularities are present. Also for FE calculations it is difficult to reach reliable results when the bending stresses become singular due to a large pollution error invading the whole domain [4][5]. Previous validations showed that the WBM suffers also from convergence problems when the stresses become singular in a corner [6][7]. A possible solution to deal with these convergence problems is to extend the set of basis functions with some additional functions. The latter functions, which will be called 'corner functions', provide an accurate representation of the singular behaviour of the problem solution near the corner point. For the hybrid Trefftz FEM, Jirousek already applied this approach to deal with corner singularities for static plate bending problems [8]. For dynamic problems, Leissa presented a procedure for determining the free vibration frequencies of sectorial plates [9]. The procedure is based on a Ritz method where the conventional set of basis functions is extended with the corner functions from the associated static problem. In this paper, the corner functions are used to resolve the convergence problems of the Trefftz-based WBM.

2 Problem definition

The basic principle of the WBM is discussed briefly for a general, coplanar plate problem. In case that the problem domain is non-convex, it must be divided in convex subdomains for convergence purposes, as shown in figure 1. Both subdomains are excited by harmonic normal point forces F_1 and F_2 . According to the thin plate theory [10], the steady-state out-of-plane displacements w_{zi} ($i = 1, 2$) are governed by the following differential equation:

$$\nabla^4 w_{zi}(x_i, y_i) - k_{bi}^4 w_{zi}(x_i, y_i) = \frac{F_i}{D_i} \delta(x_{Fi}, y_{Fi}), \quad (1)$$

where $\nabla^4 = \frac{\partial^4}{\partial x_i^4} + 2\frac{\partial^4}{\partial x_i^2 \partial y_i^2} + \frac{\partial^4}{\partial y_i^4}$. The plate bending wavenumber k_{bi} and the plate bending stiffness D_i are defined as

$$k_{bi} = \sqrt[4]{\frac{\rho_i h_i \omega^2}{D_i}} \quad \text{and} \quad D_i = \frac{E_i h_i^3}{12(1 - \nu_i^2)}, \quad (2)$$

with h_i the plate thickness, E_i the elasticity modulus, ν_i the Poisson coefficient and ρ_i the plate material density related with subdomain (i).

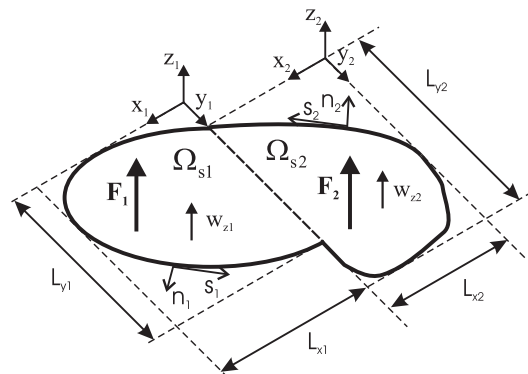


Figure 1: A general non-convex plate problem.

The following expressions represent the most commonly encountered boundary conditions at the plate boundaries $\Gamma_s^{(i)}$ ($= \Gamma_{w\theta}^{(i)} \cup \Gamma_{mQ}^{(i)} \cup \Gamma_{wm}^{(i)} \cup \Gamma_c$),

- kinematic boundary conditions: displacement and rotation are prescribed

$$\begin{aligned} R_{wi}(\mathbf{r}_i) &= w_{zi}(\mathbf{r}_i) - \bar{w}_{zi}(\mathbf{r}_i) = 0 \\ R_{\theta i}(\mathbf{r}_i) &= \mathcal{L}_\theta^{(i)}[w_{zi}(\mathbf{r}_i)] - \bar{\theta}_{ni}(\mathbf{r}_i) = 0 \quad \mathbf{r}_i \in \Gamma_{w\theta}^{(i)}, \end{aligned} \quad (3)$$

- mechanical boundary conditions: bending moment and generalised shear force are prescribed

$$\begin{aligned} R_{mi}(\mathbf{r}_i) &= \mathcal{L}_m^{(i)}[w_{zi}(\mathbf{r}_i)] - \bar{m}_{ni}(\mathbf{r}_i) = 0 \\ R_{Qi}(\mathbf{r}_i) &= \mathcal{L}_Q^{(i)}[w_{zi}(\mathbf{r}_i)] - \bar{Q}_{ni}(\mathbf{r}_i) = 0 \quad \mathbf{r}_i \in \Gamma_{mQ}^{(i)}, \end{aligned} \quad (4)$$

- mixed boundary conditions: displacement and bending moment are prescribed

$$\begin{aligned} R_{wi}(\mathbf{r}_i) &= w_{zi}(\mathbf{r}_i) - \bar{w}_{zi}(\mathbf{r}_i) = 0 \\ R_{mi}(\mathbf{r}_i) &= \mathcal{L}_m^{(i)}[w_{zi}(\mathbf{r}_i)] - \bar{m}_{ni}(\mathbf{r}_i) = 0 \quad \mathbf{r}_i \in \Gamma_{wm}^{(i)}, \end{aligned} \quad (5)$$

with \bar{w}_{zi} , $\bar{\theta}_{ni}$, \bar{m}_{ni} and \bar{Q}_{ni} the prescribed values for, respectively, the displacement, the rotational displacement, the bending moment and the generalised shear force.

Along the interface Γ_c between the two subdomains the force equilibrium and displacement compatibility lead to the following four conditions:

$$\begin{aligned} R_{mc}(\mathbf{r}_1) &= \mathcal{L}_m^{(1)}[w_{z1}(\mathbf{r}_1)] - \mathcal{L}_m^{(2)}[w_{z2}(\mathbf{r}_2)] = 0 \\ R_{Qc}(\mathbf{r}_1) &= \mathcal{L}_Q^{(1)}[w_{z1}(\mathbf{r}_1)] + \mathcal{L}_Q^{(2)}[w_{z2}(\mathbf{r}_2)] = 0 \quad \mathbf{r}_1 \in \Gamma_c, \end{aligned} \quad (6)$$

$$\begin{aligned} R_{wc}(\mathbf{r}_2) &= w_{z2}(\mathbf{r}_2) - w_{z1}(\mathbf{r}_1) = 0 \\ R_{\theta c}(\mathbf{r}_2) &= \mathcal{L}_\theta^{(2)}[w_{z2}(\mathbf{r}_2)] + \mathcal{L}_\theta^{(1)}[w_{z1}(\mathbf{r}_1)] = 0 \quad \mathbf{r}_2 \in \Gamma_c. \end{aligned} \quad (7)$$

The differential operators for, respectively, the rotational displacement, bending moment and generalised shear force are defined as follows,

$$\begin{aligned} \mathcal{L}_\theta^{(i)} &= -\frac{\partial}{\partial n_i}, \\ \mathcal{L}_m^{(i)} &= -D_i \left(\frac{\partial^2}{\partial n_i^2} + \nu_i \frac{\partial^2}{\partial s_i^2} \right), \\ \mathcal{L}_Q^{(i)} &= -D_i \frac{\partial}{\partial n_i} \left(\frac{\partial^2}{\partial n_i^2} + (2 - \nu_i) \frac{\partial^2}{\partial s_i^2} \right), \end{aligned} \quad (8)$$

where n_i and s_i are, respectively, the in-plane normal and in-plane tangential directions of the plate boundary.

3 Stress singularities

As mentioned in the introduction, stress singularities may complicate the prediction by standard numerical methods. The bending stresses often become singular in the vicinity of an angular corner. This singularity arises when the internal angle formed by the two edges of the corner exceeds a critical value. The critical value depends on the boundary conditions applied along the two adjacent edges. This section discusses the singular behaviour in the vicinity of a corner. The aim of this study is twofold. It allows to identify possible corner singularities and to define some additional basis functions for the WBM to accurately represent the singular behaviour. The stresses within a small vicinity of the corner are hardly affected by the boundary conditions away from the corner point. Therefore it is reasonable to study the behaviour near a corner by means of an infinite wedge domain, see figure 2. Provided that the internal angle and the radial boundary conditions correspond to those of the corner in the original problem, the singular behaviour near the corner will be identical in both problems. For the infinite wedge problem, an analytical solution for the out-of-plane displacement w_z is defined. This solution needs to satisfy (i) the dynamic equation, (ii) two regularity conditions in the corner point and (iii) the radial boundary conditions. Starting from the exact analytical solution, the bending moments and their singular behaviour can be evaluated.

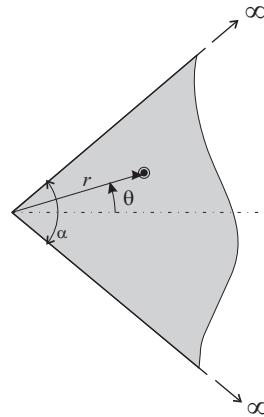


Figure 2: Infinite wedge domain.

3.1 Analytical solution

Assuming a separable function w_z and utilizing the polar coordinates as indicated in figure 2, yield the following homogeneous solution,

$$w_z = \sum_k \cos(\lambda_k \theta) R_{\lambda_k}(k_b r) + \sin(\lambda_k^* \theta) R_{\lambda_k^*}(k_b r), \quad (9)$$

with

$$R_{\lambda}(k_b r) = A_{\lambda} J_{\lambda}(k_b r) + B_{\lambda} Y_{\lambda}(k_b r) + C_{\lambda} I_{\lambda}(k_b r) + D_{\lambda} K_{\lambda}(k_b r), \quad \lambda = \lambda_k \vee \lambda_k^* \quad (10)$$

and with $A_{\lambda}, \dots, D_{\lambda}$ 4 constants of integration and with $J_{\lambda}, Y_{\lambda}, I_{\lambda}$ and K_{λ} the ordinary and modified Bessel functions of the first and second kind. The eigenfunctions associated with λ_k describe the symmetric bending with respect to the axis $\theta = 0$; the ones associated with λ_k^* are anti-symmetric with respect to this axis. The eigenvalues λ_k and λ_k^* are solutions of the characteristic determinant arising from applying the radial boundary conditions.

The four integration constants of each eigenfunction are determined by imposing independent equations for $r = \infty$ and $r = 0$. The conditions at infinity do not influence the singular behaviour and are not considered therefore. At the corner two regularity conditions are imposed,

$$w_z(0, \theta) = \text{finite}, \quad (11)$$

$$\frac{\partial w_z}{\partial r}(0, \theta) = \text{finite}. \quad (12)$$

The regularity conditions lead to the following relations between the integration constants:

$$\lambda < 1 \quad \begin{cases} B_{\lambda} - \frac{\pi}{2} D_{\lambda} = 0, \\ A_{\lambda} + \frac{\cos(\lambda-1)\pi}{\sin(\lambda-1)\pi} B_{\lambda} + C_{\lambda} + \frac{\pi}{2 \sin(\lambda-1)\pi} D_{\lambda} = 0. \end{cases} \quad (13)$$

$$\lambda > 1 \quad \begin{cases} B_{\lambda} = 0, \\ D_{\lambda} = 0, \end{cases} \quad (14)$$

Thus, imposing the two regularity conditions at the corner results in the following eigenfunctions:

$$\lambda < 1 \quad R_{\lambda} = A_{\lambda} \left(J_{\lambda}(k_b r) - C Y_{\lambda}(k_b r) - \frac{2}{\pi} C K_{\lambda}(k_b r) \right) + C_{\lambda} \left(I_{\lambda}(k_b r) - C Y_{\lambda}(k_b r) - \frac{2}{\pi} C K_{\lambda}(k_b r) \right) \quad (15)$$

$$\lambda > 1 \quad R_{\lambda} = A_{\lambda} J_{\lambda}(k_b r) + C_{\lambda} I_{\lambda}(k_b r), \quad (16)$$

with $C = \frac{\sin(\lambda-1)\pi}{\cos(\lambda-1)\pi+1}$ and with $\lambda = \lambda_k \vee \lambda_k^*$ depending on whether λ is associated with a symmetric or anti-symmetric eigenfunction.

3.2 Bending moment singularities

Now that an exact analytical solution (9) for the displacement field w_z is defined, it is possible to evaluate the bending moments in the vicinity of the corner point. The circumferential bending moment m_θ is given by,

$$m_\theta = -D \left(\frac{1}{r} \frac{\partial w_z}{\partial r} + \frac{1}{r^2} \frac{\partial^2 w_z}{\partial \theta^2} + \nu \frac{\partial^2 w_z}{\partial r^2} \right). \tag{17}$$

Substituting the eigenfunction R_λ in this equation for $\lambda > 1$ and using the known Bessel functions relations [11] results in,

$$\begin{aligned} m_\theta = & \left(A_\lambda \left\{ \frac{\nu k_b^2}{4} J_{\lambda-2}(k_b r) + \frac{k_b}{2r} J_{\lambda-1}(k_b r) - \left(\frac{\nu k_b^2}{2} + \frac{\lambda^2}{r^2} \right) J_\lambda(k_b r) \right. \right. \\ & \left. \left. - \frac{k_b}{2r} J_{\lambda+1}(k_b r) + \frac{\nu k_b^2}{4} J_{\lambda+2}(k_b r) \right\} \right. \\ & \left. + C_\lambda \left\{ \frac{\nu k_b^2}{4} I_{\lambda-2}(k_b r) + \frac{k_b}{2r} I_{\lambda-1}(k_b r) + \left(\frac{\nu k_b^2}{2} - \frac{\lambda^2}{r^2} \right) I_\lambda(k_b r) \right. \right. \\ & \left. \left. + \frac{k_b}{2r} I_{\lambda+1}(k_b r) + \frac{\nu k_b^2}{4} I_{\lambda+2}(k_b r) \right\} \right). \tag{18} \end{aligned}$$

Using the power series of the Bessel functions [11], the circumferential bending moment in the vicinity of the corner point can be expressed as follows,

$$m_\theta|_{r=0} = \lim_{r \rightarrow 0} \left(\frac{\nu}{\Gamma(\lambda-1)} + \frac{1}{\Gamma(\lambda)} - \frac{\lambda^2}{\Gamma(\lambda+1)} \right) r^{\lambda-2}, \quad \lambda > 1. \tag{19}$$

Eq. (19) shows that the circumferential bending moment associated with the eigenfunction R_λ becomes singular in the corner point when $\lambda < 2$. The order of the singularity is $\lambda - 2$.

The same is done for eigenvalues $\lambda < 1$. Substituting the eigenfunction (15) in the expression for the bending moment (17) and using the Bessel function relations and power series expansions leads to the following expression for the bending moment,

$$m_\theta|_{r=0} = \lim_{r \rightarrow 0} \left(\frac{2}{\sin \lambda \pi} \frac{1}{\Gamma(1-\lambda)} + \frac{1}{\sin \lambda \pi} \frac{1}{\Gamma(-\lambda)} \right) r^{-\lambda}, \quad \lambda < 1. \tag{20}$$

In this case the bending moments are singular for the entire range of λ , that is $0 < \lambda < 1$ and the order of the singularity is $-\lambda$. In conclusion, it is shown that an eigenfunction will give rise to a singular bending moment when its associated eigenvalue λ is smaller than two.

The order of the singularities in the radial bending moment and twisting moment are identical to that of the circumferential bending moment.

3.3 Simply supported infinite wedge

The eigenvalues λ are determined by the radial boundary conditions. However, it is only possible to define an exact solution satisfying the radial boundary conditions if both radial edges are simply supported. In this case, the following boundary conditions are applied,

$$w_z(r, \pm \frac{\alpha}{2}) = 0, \tag{21}$$

$$m_n(r, \pm \frac{\alpha}{2}) = 0. \tag{22}$$

The eigenvalues result from applying the boundary conditions to the homogeneous solution (9) and solving the resulting characteristic determinant,

$$\lambda_k = (2k - 1) \frac{\pi}{\alpha} \quad k = 1, 2, \dots, \quad (23)$$

$$\lambda_k^* = \frac{2k\pi}{\alpha} \quad k = 1, 2, \dots. \quad (24)$$

In the previous section it was demonstrated that the bending moments become singular if one of the eigenvalues becomes smaller than two. For the simply supported infinite wedge, this implies that singular bending moments occur whenever the internal angle exceeds $\pi/2$. In this case, the first symmetric eigenvalue $\lambda_1 = \pi/\alpha$ becomes smaller than two, thereby invoking a singularity in the bending moments. The anti-symmetric eigenfunctions only introduce singularities when the internal angle exceeds π . The eigenfunctions and eigenvalues as defined here, form an exact analytical solution since they satisfy the dynamic equations, the regularity conditions and the radial boundary conditions. Consequently, they represent the exact singular behaviour around the corner and can be included as corner functions in the WBM.

It is interesting to compare the previously defined dynamic solution with the solution of the corresponding static problem. For static plate problems, the analytical solutions were originally defined by Williams [12],

$$w_z = \sum_s r^{\lambda_s+1} \{A_{\lambda_s} \cos(\lambda_s + 1)\theta + B_{\lambda_s} \cos(\lambda_s - 1)\theta\} + r^{\lambda_s^*+1} \{A_{\lambda_s^*} \sin(\lambda_s^* + 1)\theta + B_{\lambda_s^*} \sin(\lambda_s^* - 1)\theta\}, \quad (25)$$

with A_λ and B_λ arbitrary constants of integration and λ_s and λ_s^* the static eigenvalues. The eigenvalues are derived such that the radial boundary conditions along $\theta = \pm \frac{\alpha}{2}$ are satisfied. Eigenvalues with a negative real part are excluded since they introduce a singularity in the slope $\frac{\partial w_z}{\partial r}$, which is in violation with the second regularity condition (12). For simply supported edges this results in,

$$\lambda_s = \frac{(2s - 1)\pi}{\alpha} \pm 1 \quad s = 1, 2, \dots, \quad (26)$$

$$\lambda_s^* = \frac{2s\pi}{\alpha} \pm 1 \quad s = 0, 1, 2, \dots. \quad (27)$$

An eigenvalue $\lambda_s = 0$ leads to the trivial solution except when the internal angle α equals π . For $\lambda_s = 1$ the system has a trivial solution except when α equals $\pi/2, \pi$ or $3\pi/2$. For an internal angle $\alpha > \pi$, there exists an additional eigenvalue

$$\lambda_s' = -\frac{\pi}{\alpha} + 1. \quad (28)$$

Since the bending moments imply a second order derivative with respect to r , the moments around the corner point behave as r^{λ_s-1} for a static problem. For the comparison between the bending moments of the static and dynamic problem, the cases $\alpha < \pi$ and $\alpha > \pi$ are considered separately:

- If the interior angle α is smaller than π , the dynamic eigenvalues are all greater than one, so that the dynamic eigenfunctions are defined as in Eq. (16). The dynamic bending moments behave as r^{λ_k-2} in the direct vicinity of the corner, see Eq. (19). The static bending moments behave as r^{λ_s-1} . Table 1 gives the smallest eigenvalues that invoke singular bending moments for both the static and dynamic problem. It can be seen that the dynamic eigenvalues λ_k correspond with $\lambda_s + 1$, both for the symmetric and anti-symmetric eigenfunctions. Thus, the static and dynamic bending moments have the same asymptotic behaviour in the vicinity of the corner point.
- If the interior angle α is larger than π , there is an additional static eigenvalue (28). The associated bending moments vary as $r^{\lambda_s'-1}$. The first dynamic, symmetric eigenvalue π/α becomes smaller than one. Hence the associated eigenfunction takes the form of Eq. (15). As shown in (20), the dynamic bending moments behave as $r^{-\lambda_k}$. The static and dynamic bending moments associated with this

	symmetric	anti-symmetric
static	$\frac{\pi}{\alpha} - 1$	$\frac{2\pi}{\alpha} - 1$
dynamic	$\frac{\pi}{\alpha}$	$\frac{2\pi}{\alpha}$

Table 1: Comparison of dynamic and static eigenvalues for $\alpha < \pi$.

eigenvalue are equivalent if $\lambda_k = 1 - \lambda'_s$, which is indeed the case. The smallest static eigenvalues of Eq. (26) and Eq. (27) are compared with the remaining dynamic eigenvalues of Eq. (23) and Eq. (24) in table 2. The anti-symmetric eigenvalues remain identical to those for $\alpha < \pi$. For the symmetric functions, the smallest static eigenvalue changes since the first value becomes negative and therefore needs to be excluded. Comparing the bending moments for these functions shows that they are still asymptotically identical in the vicinity of the corner.

	symmetric	anti-symmetric
static	$\frac{3\pi}{\alpha} - 1$	$\frac{2\pi}{\alpha} - 1$
dynamic	$\frac{3\pi}{\alpha}$	$\frac{2\pi}{\alpha}$

Table 2: Comparison of dynamic and static eigenvalues for $\alpha > \pi$.

In summary, the asymptotic behaviour of the bending moments in the vicinity of the corner is identical for the static and dynamic solutions.

3.4 Other radial boundary conditions

When the two radial edges are not both simply supported, it is no longer possible to define an exact analytical solution. This is a consequence of the fact that the solution is not separable in variables. Leissa demonstrated in [13] that the nodal patterns of sectorial plates do not consist of nodal radii or circles for other boundary conditions than simply supported. For static problems, on the other hand, the analytical solutions for each possible combination of radial boundary conditions are defined by Williams [12]. Leissa incorporates the static eigenfunctions in a Ritz method to determine the free vibration frequencies of sectorial plates [9]. However, since the WBM is an indirect Trefftz method and thus requires basis functions that a priori satisfy the dynamic equations, it is impossible to incorporate the Williams functions as basis functions. Only functions consistent with Eq. (9) satisfy the homogeneous, dynamic plate equation and can be included as basis functions in the WBM. The characteristic eigenvalues λ that should follow from the radial boundary conditions, will now be chosen such that the singular behaviour around the corner is asymptotically the same as that of the corresponding static solution. As derived in the previous section for the simply supported case, it is assumed that the static and dynamic solutions for other combinations of radial boundary conditions have also the same asymptotic behaviour around the corner point if,

$$\lambda = \lambda_s + 1. \tag{29}$$

The eigenfunctions are defined as in Eq. (16). For the additional static eigenvalues as in Eq. (28), the bending moments are asymptotically identical if,

$$\lambda = 1 - \lambda'_s. \tag{30}$$

These dynamic eigenvalues will be smaller than one; the corresponding eigenfunctions are thus defined according to Eq. (15). The resulting eigenfunctions satisfy the dynamic equation inherently. Although the radial boundary conditions will not be satisfied, the singularities near the corner will be taken into account in an asymptotically correct way.

4 Basic concepts of the Wave Based Method

This section describes the basic principles of the WBM for a non-convex plate domain, as defined in section 2. In contrast with the FEM, the WBM is an indirect Trefftz method. The WBM divides the plate domain into a small number of subdomains. As long as the subdomains are convex, the convergence of the method is ensured. Within each subdomain, the field variables are described with an expansion of basis functions which satisfy the governing dynamic equations exactly. In this way, there is only an approximation error induced in the boundary and interface conditions. Minimising this approximation error in an integral sense leads to the solution of the system.

4.1 Field variable expansion

The steady-state displacement w_{zi} in subdomain (i) is approximated as a solution expansion of two sets,

$$w_{zi} \approx \hat{w}_{zi} = \hat{w}_{zi}^T + \sum_{c_i} \hat{w}_{zci}^C. \quad (31)$$

The first set \hat{w}_{zi}^T comprises the conventional wave functions that are solutions of the dynamic equations. This set forms a complete set, thereby ensuring convergence to the exact result. However, when the bending stresses become singular in a corner, a prohibitively high number of wave functions is needed. Enriching the expansion with some additional functions that accurately represent the singular behaviour around that corner can accelerate the convergence. Therefore, the set of wave functions is extended with a second set \hat{w}_{zci}^C that contains corner functions for each corner point (c_i) of the considered subdomain (i) where the stresses become singular. Each of these functions is defined in their proper coordinate system.

4.1.1 Wave functions

The first set of the solution expansion consists of the wave functions and is defined as follows,

$$\hat{w}_{zi}^T(\mathbf{r}_i) = \sum_{b=1}^{n_{bi}} w_{bi}^T \Psi_{bi}(\mathbf{r}_i) + \hat{w}_{Fi}(\mathbf{r}_i) = [\Psi_{bi}] \{w_{bi}^T\} + \hat{w}_{Fi}(\mathbf{r}_i), \quad (32)$$

in which each wave function Ψ_{bi} satisfies the homogeneous part of the dynamic equation (1). The wave functions that satisfy the homogeneous differential equation, are divided into two different sets as indicated in table 3. The selection of the wavenumbers $k_{b,x}^{(i)}$ and $k_{b,y}^{(i)}$ is based on the dimensions ($L_{xi} \times L_{yi}$) of the preferably smallest rectangular box circumscribing subdomain (i), see figure 1. The first wavenumber, $k_{b,x}^{(i)}$ or $k_{b,y}^{(i)}$, is chosen such that an integer number of half wavelengths equals the length of the rectangular box in the corresponding direction. The other component of the wavenumber is calculated from the structural wavenumber k_{bi} at the considered frequency. For the first set of wave functions, the functions associated with the first wavenumber are cosine functions. For the second set, the functions associated with the first wavenumber are sine functions. It has been proven by Desmet in [14] that the first set of wave functions is capable of representing any displacement field provided that the domain is convex, and thus that the convergence of the WBM is theoretically guaranteed. In case of a non-convex plate domain, it must be divided into convex subdomains to ensure convergence.

The number of bending wave functions n_{bi} that is included in expansion (32) is related to the excitation frequency and the dimensions of the enclosing rectangular box,

$$n_{bi} = 4(n_{b1i} + 1) + 4(n_{b2i} + 1) + 4n_{b3i} + 4n_{b4i}, \quad (33)$$

with,

$$\frac{n_{b1i}}{L_{xi}} \approx \frac{n_{b2i}}{L_{yi}} \approx \frac{n_{b3i}}{L_{xi}} \approx \frac{n_{b4i}}{L_{yi}} \geq T_1 \frac{k_{bi}}{\pi}, \quad (34)$$

with $n_{b_1i}, n_{b_2i}, n_{b_3i}$ and n_{b_4i} integer truncation values and with T_1 a user defined parameter. In this way the largest wavenumber of the bending wave functions included in the model is at least T_1 times the structural wavenumber at the considered frequency.

set	wave functions	wavenumbers
1	$\Psi_{b_1i}(x_i, y_i) = \cos(k_{b_1,x}^{(i)}x_i) \exp(-jk_{b_1,y}^{(i)}y_i)$	$k_{b_1,x}^{(i)} = \frac{b_1\pi}{L_{x_i}}, \quad k_{b_1,y}^{(i)} = \begin{cases} \pm\sqrt{k_{b_i}^2 - \left(\frac{b_1\pi}{L_{x_i}}\right)^2} \\ \pm j\sqrt{k_{b_i}^2 + \left(\frac{b_1\pi}{L_{x_i}}\right)^2} \end{cases}$ $b_1=0,1,\dots,n_{b_1i}$
	$\Psi_{b_2i}(x_i, y_i) = \exp(-jk_{b_2,x}^{(i)}x_i) \cos(k_{b_2,y}^{(i)}y_i)$	$k_{b_2,y}^{(i)} = \frac{b_2\pi}{L_{y_i}}, \quad k_{b_2,x}^{(i)} = \begin{cases} \pm\sqrt{k_{b_i}^2 - \left(\frac{b_2\pi}{L_{y_i}}\right)^2} \\ \pm j\sqrt{k_{b_i}^2 + \left(\frac{b_2\pi}{L_{y_i}}\right)^2} \end{cases}$ $b_2=0,1,\dots,n_{b_2i}$
2	$\Psi_{b_3i}(x_i, y_i) = \sin(k_{b_3,x}^{(i)}x_i) \exp(-jk_{b_3,y}^{(i)}y_i)$	$k_{b_3,x}^{(i)} = \frac{b_3\pi}{L_{x_i}}, \quad k_{b_3,y}^{(i)} = \begin{cases} \pm\sqrt{k_{b_i}^2 - \left(\frac{b_3\pi}{L_{x_i}}\right)^2} \\ \pm j\sqrt{k_{b_i}^2 + \left(\frac{b_3\pi}{L_{x_i}}\right)^2} \end{cases}$ $b_3=1,\dots,n_{b_3i}$
	$\Psi_{b_4i}(x_i, y_i) = \exp(-jk_{b_4,x}^{(i)}x_i) \sin(k_{b_4,y}^{(i)}y_i)$	$k_{b_4,y}^{(i)} = \frac{b_4\pi}{L_{y_i}}, \quad k_{b_4,x}^{(i)} = \begin{cases} \pm\sqrt{k_{b_i}^2 - \left(\frac{b_4\pi}{L_{y_i}}\right)^2} \\ \pm j\sqrt{k_{b_i}^2 + \left(\frac{b_4\pi}{L_{y_i}}\right)^2} \end{cases}$ $b_4=1,\dots,n_{b_4i}$

Table 3: Sets of wave functions.

Function \hat{w}_{Fi} is a particular solution function to take into account the inhomogeneous part of the dynamic equation that arises from the external excitation applied on the plate. From all possible mathematical expressions, the displacement of an infinite plate excited by a normal point force is selected,

$$\hat{w}_{Fi}(\mathbf{r}_i) = -\frac{jF_i}{8k_{b_i}^2 D_i} \left[H_0^{(2)}(k_{b_i} r_{Fi}) - H_0^{(2)}(-jk_{b_i} r_{Fi}) \right] \tag{35}$$

$$\text{with } r_{Fi} = \sqrt{(x_i - x_{Fi})^2 + (y_i - y_{Fi})^2}, \tag{36}$$

and where $H_0^{(2)}$ is the zero-order Hankel function of the second kind.

4.1.2 Corner functions

In the case of stress singularities, the set of wave functions is extended with a second set of corner functions. For each corner (c) of the plate in which singular stresses occur, a number of corner functions Υ_{bc} associated with that corner are added,

$$\hat{w}_{zci}^C = \sum_{b=1}^{n_c} w_{bc}^C \Upsilon_{bc}^{(i)}(r_c, \theta_c) \tag{37}$$

with n_c the number of included corner functions for that corner and (i) the subdomain to which the corner belongs. Each corner function is defined in a coordinate system with the corner as origin and θ related to the bisecting line, see figure 3. In contrast with the wave functions, which are defined within one subdomain, the corner functions are related to a corner and are not necessarily restricted to one subdomain. In case that the corner point lies on a interface, and thus belongs to several subdomains, the functions associated with that corner extent over the different subdomains adjacent to that corner. For example, corner c_2 in figure 3

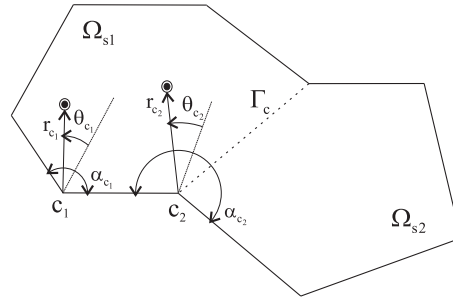


Figure 3: Definition of corner functions.

belongs to both subdomain Ω_{s1} and Ω_{s2} . Thus the corner functions associated with this corner extend over the two subdomains. For corner c_1 on the other hand, the corner functions are only defined in subdomain Ω_{s1} . The eigenvalues λ_{bc} or λ_{bc}^* of a corner function depend on the type of singularity and thus on the boundary conditions along the adjacent edges and the interior angle α_c of the corresponding corner. When the eigenvalue is larger than one, the corner functions are defined as follows,

$$\Upsilon_{bc}^{(i)}(r_c, \theta_c) = \begin{cases} \cos \lambda_{bc} \theta_c J_{\lambda_{bc}}(k_{bi} r_c), \\ \cos \lambda_{bc} \theta_c I_{\lambda_{bc}}(k_{bi} r_c), \\ \sin \lambda_{bc}^* \theta_c J_{\lambda_{bc}^*}(k_{bi} r_c), \\ \sin \lambda_{bc}^* \theta_c I_{\lambda_{bc}^*}(k_{bi} r_c). \end{cases} \quad (38)$$

When the characteristic value is smaller than one, the corner functions are defined as,

$$\Upsilon_{bc}^{(i)}(r_c, \theta_c) = \begin{cases} \cos \lambda_{bc} \theta_c \left(J_{\lambda_{bc}}(k_{bi} r_c) - C_{bc} Y_{\lambda_{bc}}(k_{bi} r_c) - \frac{2}{\pi} C_{bc} K_{\lambda_{bc}}(k_{bi} r_c) \right), \\ \cos \lambda_{bc} \theta_c \left(I_{\lambda_{bc}}(k_{bi} r_c) - C_{bc} Y_{\lambda_{bc}}(k_{bi} r_c) - \frac{2}{\pi} C_{bc} K_{\lambda_{bc}}(k_{bi} r_c) \right), \\ \sin \lambda_{bc}^* \theta_c \left(J_{\lambda_{bc}^*}(k_{bi} r_c) - C_{bc}^* Y_{\lambda_{bc}^*}(k_{bi} r_c) - \frac{2}{\pi} C_{bc}^* K_{\lambda_{bc}^*}(k_{bi} r_c) \right), \\ \sin \lambda_{bc}^* \theta_c \left(I_{\lambda_{bc}^*}(k_{bi} r_c) - C_{bc}^* Y_{\lambda_{bc}^*}(k_{bi} r_c) - \frac{2}{\pi} C_{bc}^* K_{\lambda_{bc}^*}(k_{bi} r_c) \right), \end{cases} \quad (39)$$

with,

$$C_{bc} = \frac{\sin(\lambda_{bc} - 1)\pi}{\cos(\lambda_{bc} - 1)\pi + 1} \quad \text{and} \quad C_{bc}^* = \frac{\sin(\lambda_{bc}^* - 1)\pi}{\cos(\lambda_{bc}^* - 1)\pi + 1}. \quad (40)$$

When both edges are simply supported, the exact analytical solution is available and the eigenvalues are defined as in Eq. (23) and Eq. (24). For other combinations of boundary conditions, the eigenvalues are determined from those of the corresponding static problem, as explained in section 3.4. Since the only objective of the corner functions is to accurately represent the singularities in the solution, only the eigenfunctions that give rise to singularities need to be included in the model.

4.2 Evaluation of boundary and interface conditions

The field variable expansion (31) satisfies the governing dynamic equations (1) exactly, irrespective of the unknown wave function contribution factors w_{bi}^T and w_{bc}^C . These contribution factors are determined by minimising the approximation errors of the boundary and interface conditions through a weighted residual formulation. The approximation errors on boundary and interface conditions of the two subdomains depicted in figure1, are orthogonalised with respect to weighting functions \tilde{w}_{z1} and \tilde{w}_{z2} respectively,

$$\begin{aligned} & \int_{\Gamma_{w\theta}^{(1)} \cup \Gamma_{wm}^{(1)}} \mathcal{L}_Q^{(1)}[\tilde{w}_{z1}] R_{w1} d\Gamma + \int_{\Gamma_{w\theta}^{(1)}} \mathcal{L}_m^{(1)}[\tilde{w}_{z1}] R_{\theta1} d\Gamma - \int_{\Gamma_{wm}^{(1)} \cup \Gamma_{mQ}^{(1)}} \mathcal{L}_\theta^{(1)}[\tilde{w}_{z1}] R_{m1} d\Gamma \\ & - \int_{\Gamma_{mQ}^{(1)}} \tilde{w}_{z1} R_{Q1} d\Gamma - \int_{\Gamma_c} \mathcal{L}_\theta^{(1)}[\tilde{w}_{z1}] R_{mc} d\Gamma - \int_{\Gamma_c} \tilde{w}_{z1} R_{Qc} d\Gamma = 0, \end{aligned} \quad (41)$$

$$\begin{aligned}
& \int_{\Gamma_{w\theta}^{(2)} \cup \Gamma_{wm}^{(2)}} \mathcal{L}_Q^{(2)}[\tilde{w}_{z2}] R_{w2} d\Gamma + \int_{\Gamma_{w\theta}^{(2)}} \mathcal{L}_m^{(2)}[\tilde{w}_{z2}] R_{\theta2} d\Gamma - \int_{\Gamma_{wm}^{(2)} \cup \Gamma_{mQ}^{(2)}} \mathcal{L}_\theta^{(2)}[\tilde{w}_{z2}] R_{m2} d\Gamma \\
& - \int_{\Gamma_{mQ}^{(2)}} \tilde{w}_{z2} R_{Q2} d\Gamma + \int_{\Gamma_c} \mathcal{L}_Q^{(2)}[\tilde{w}_{z2}] R_{wc} d\Gamma + \int_{\Gamma_c} \mathcal{L}_m^{(2)}[\tilde{w}_{z2}] R_{\theta c} d\Gamma = 0.
\end{aligned} \tag{42}$$

As mentioned before, the corner functions are not necessarily restricted to one subdomain. In case that a function is defined in two subdomains, it will not give rise to an approximation error over the interface between the two subdomains since the continuity is a priori guaranteed. The corner function will therefore be excluded from the residuals over that interface. The weighting functions are chosen in a similar way as in the Galerkin weighting procedure. In this way a square system of equations in the unknown contribution factors w_{bi}^T and w_{bc}^C is obtained.

4.3 Model properties

Both the FEM and the WBM are deterministic prediction techniques, however they are based on a completely different concept. The FEM is based on the Rayleigh-Ritz principle, whereas the WBM is a Trefftz approach. Compared with the FEM, the WBM has the following advantages:

- Compared to the FE models, the WB models are substantially smaller. Thanks to the smaller system matrices and the subsequent smaller computational load, the WBM becomes applicable at higher frequencies.
- The spatial derivatives of the wave functions are also wave functions, such that the derived variables have the same spatial resolution as the primary variable. For the FEM, the derived variables are less accurate since the basisfunctions are usually polynomial functions.
- To refine the WB models, an additional number of wave functions is included. This results in the addition of a number of matrix elements while the original elements remain unaltered. For the FEM a global model refinement requires a new model calculation.

The disadvantages of the WBM include the following:

- The WB system matrices are fully populated and contain complex valued elements. In addition, the WB models suffer from a poor numerical condition. The ill-conditioning does not prevent the practical convergence of the WBM but it requires that all computations are performed with a high accuracy.
- It is not possible to decompose the WB models into frequency independent matrices, such that the system matrix needs to be calculated at each frequency of interest.
- A major advantage of the FEM is that it is widely applicable. There are hardly any restrictions on the geometric complexity of the problem. The application of the WBM, on the other hand, is restricted to problems of only moderate geometric complexity to benefit from its enhanced computational efficiency.

5 Validation examples

In this section the computational advantages of the WBM are demonstrated for two validation examples. For convex problems, including only the wave functions of the first set that guarantee theoretical convergence, see section 4.1.1, is optimal for the convergence rate [7]. It is shown here that this is not valid for non-convex problems. Furthermore, the performance of the WBM is compared with the FEM. This comparison

is made both on accuracy as on computation time. All FE predictions are calculated using MSC/Nastran2004, whereas the WBM is implemented in C++. The FE predictions include both a linear 4-noded and a quadratic 8-noded quadrilateral shell discretisation. All FE predictions use a direct solution method. For the computation time of the FEM only the direct solving time is included, since the FE models can be decomposed into frequency independent matrices. For the WBM, on the other hand, the computation time includes both the time needed for constructing the model as well as the time needed for solving the model. All calculations were performed on a 3GHz Intel Pentium 4 processor running a Linux operation system.

5.1 U-shaped plate

A first example consists of a U-shaped plate. Since the problem domain is non-convex, it must be divided into convex subdomains. The domain decomposition is indicated in figure 4. All the plate boundaries are simply supported. The plate is made of aluminium ($E = 70 \cdot 10^9 N/m^2$, $\nu = 0.3$, $\rho = 2790 kg/m^3$) and has a thickness of 0.002m. A unit normal point force is applied to the first subdomain at position $(x_F, y_F) = (0.15m, 0.15m)$. The three response points are located at $w_1(0.5m, 0.1m)$, $w_2(0.6m, 0.35m)$ and $w_3(0.2m, 0.65m)$.

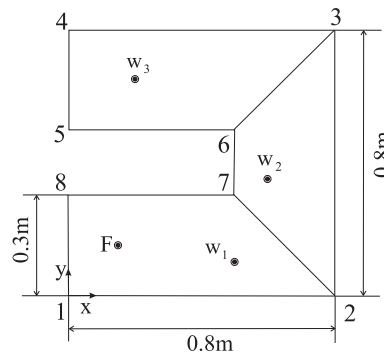


Figure 4: U-shaped plate.

corner	angle	eigenfunction	eigenvalue
c	270°	$\Upsilon_{1,c} = \cos(\lambda_{1,c}\theta) \left(J_{\lambda_{1,c}}(k_b r) - C_{1,c} Y_{\lambda_{1,c}}(k_b r) - \frac{2}{\pi} C_{1,c} K_{\lambda_{1,c}}(k_b r) \right)$ $\Upsilon_{2,c} = \cos(\lambda_{1,c}\theta) \left(I_{\lambda_{1,c}}(k_b r) - C_{1,c} Y_{\lambda_{1,c}}(k_b r) - \frac{2}{\pi} C_{1,c} K_{\lambda_{1,c}}(k_b r) \right)$ $\Upsilon_{3,c} = \sin(\lambda_{1,c}^* \theta) J_{\lambda_{1,c}^*}(k_b r)$ $\Upsilon_{4,c} = \sin(\lambda_{1,c}^* \theta) I_{\lambda_{1,c}^*}(k_b r)$	$\lambda_{1,c} = 0.66667$ $\lambda_{1,c}^* = 1.33333$

Table 4: Eigenfunctions and eigenvalues for the U-shaped plate (c=6,7).

In case that the radial edges are simply supported, the stresses in the corner points are evaluated by using the exact analytical solutions of an infinite wedge. As stated in section 3.3, singularities can be expected if the interior angle exceeds $\pi/2$. For the U-shape, this implies that there will be singularities in the corners 6 and 7 and that convergence problems can be expected for the conventional WBM implementation without corner functions. This is confirmed by figure 5. This figure shows the displacement in response point w_3 predicted with the WBM with and without corner functions. The results are compared with the results of a FE model with 408,153 degrees of freedom. The structural wavelength λ_b equals 0.178m at 600Hz, where the largest element size of the FE model is 0.0028m. The bottom figure gives the prediction of the WBM without corner functions. The model includes wave functions of both sets and uses a truncation rule $T_1 = 1.5$. As expected,

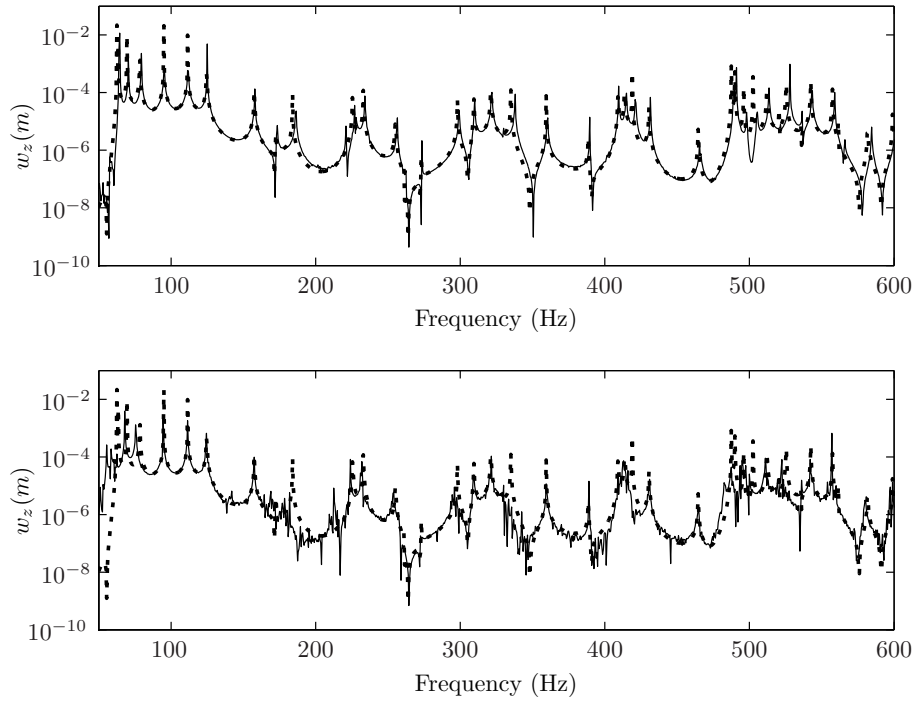


Figure 5: Frequency response function for response point w_3 (dashed: FE reference 408,153dofs / solid: WBM CF set1+2(top), WBM set1+2 (bottom)).

the WBM suffers from convergence problems, which prevent convergence to the correct result at several frequencies. In a second WB model, the set of wave functions is extended with some corner functions for corners 6 and 7. The corner functions for each of these corners are summarised in table 4. The included wave functions are identical to those of the first model. The prediction of the WB model with corner functions is shown in the top figure. The WBM suffers no longer from any convergence problems and achieves a good accuracy compared with the reference result.

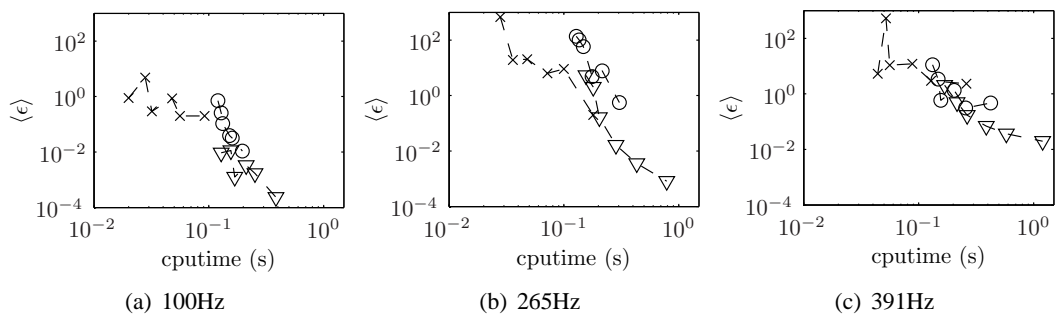


Figure 6: Convergence curves for the WBM ($- \times -$ set1 / $- \circ -$ CF set1 / $- \nabla -$ CF set1+2).

frequency (Hz)	# wave functions set 1 per subdomain	# wave functions set 2 per subdomain	# corner functions
100	112	104	8
265	176	168	8
391	212	204	8

Table 5: WB reference models for the U-shaped plate.

Figure 6 plots the convergence rate of the WBM. The figure plots the relative prediction error on the displacement as a function of the CPU time. The prediction error is averaged over the $n_{rp} = 3$ response points,

$$\langle \epsilon \rangle = \frac{1}{n_{rp}} \sum_{j=1}^{n_{rp}} \epsilon_j, \quad (43)$$

with,

$$\epsilon_j = \frac{\|w_z(\mathbf{r}_j) - w_z^{ref}(\mathbf{r}_j)\|}{\|w_z^{ref}(\mathbf{r}_j)\|}. \quad (44)$$

The results of three different WB models are included,

- only wave functions of the first set (*set1*),
- only wave functions of the first set and corner functions (*CF set1*),
- wave functions of both the first and second set and corner functions (*CF set1+2*).

As reference a WB model with wave functions of both sets and corner functions is used. The WB reference model sizes are indicated in table 5. The accuracy of the conventional WBM (*set1*) is rather poor. The models with corner functions on the other hand, achieve a good accuracy. However, it is also seen that including Bessel functions in the expansion substantially increases the computation time. Furthermore, it seems that including the wave functions of the second set has a beneficial effect on the convergence. This result is in contrast with that of the convex plate, where the functions of the second set had no influence on the convergence rate. As the WBM (*CF set1+2*) achieves the highest convergence rate, it has been used for subsequent predictions.

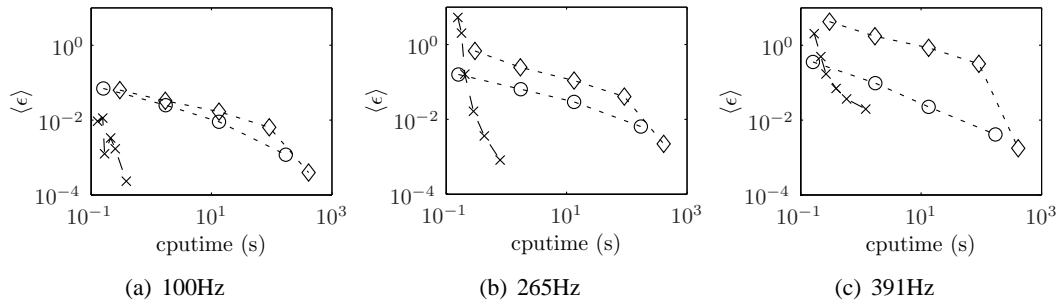


Figure 7: Convergence curves (— × — WBM CF set1+2 /— ◊ — FEM linear /— o — FEM quadratic).

frequency (Hz)	wavelength λ_b (m)	# FE dofs	element size (m)
100	0.436	3,387,759	0.0017
265	0.268	3,387,759	0.0017
391	0.221	3,387,759	0.0017

Table 6: FE reference models for the U-shaped plate.

The convergence rate of the WBM (*CF set1+2*) and FEM are compared in figure 7. These figures plot again the averaged relative prediction error as a function of the CPU time. For the FEM, both the predictions of a 4-noded linear and a 8-noded quadratic element discretisation are included and a quadratic FE model of 3,387,759 degrees of freedom is used as reference, see table 6. For the WB predictions the WB reference model is used, see table 5. The WBM has clearly an enhanced convergence rate compared with the FEM, even if quadratic elements are used.

5.2 Hexagonal plate

A second validation example consists of a hexagonal plate with a side length of $0.5m$ and with a central square cut out. The structure has a thickness of $0.0005m$ and is made of aluminium ($E = 70 \cdot 10^9 N/m^2$, $\nu = 0.3$, $\rho = 2790kg/m^3$). All plate boundaries are clamped. Again the problem domain is non-convex so that the domain must be divided into subdomains. Figure 8 shows the problem geometry and the subdomain division. The structure is excited by a unit normal point force applied at $(x_F, y_F) = (0.05m, 0.3m)$ and the result will be calculated in the following response points, $w_1(-0.05m, 0.2m)$, $w_2(0.3m, 0.02m)$, $w_3(0.06m, -0.3m)$ and $w_4(-0.3m, -0.06m)$.

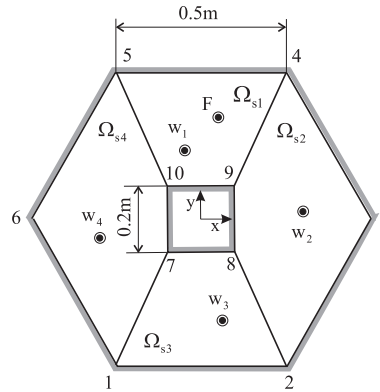


Figure 8: Hexagonal plate.

Also in this example singular bending moments are expected in the corners. In absence of the exact analytical solutions for the dynamic problem, the eigenvalues of the corresponding static problem are used. The characteristic equations for a static clamped-clamped infinite wedge are given by [12],

$$\sin \lambda_s \alpha = -\lambda_s \sin \alpha, \quad (45)$$

$$\sin \lambda_s^* \alpha = \lambda_s^* \sin \alpha, \quad (46)$$

for, respectively, the symmetric and anti-symmetric eigenfunctions. An eigenvalue $\lambda = 0$ yields the trivial solution. An eigenvalue $\lambda = 1$ yields the trivial solution except when the internal angle α equals $257, 45^\circ$ or π . In general, the eigenvalues will be complex. But since only the real part of the eigenvalues introduces singularities, only the real part will be considered. The non-linear equations (45) and (46) are solved in Matlab using the Powell dogleg method described in [15]. The characteristic equations indicate that singularities can be expected if the internal angle exceeds π . For the hexagonal plate there are thus four corners where singularities occur, $c = 7 - 10$. The dynamic eigenfunctions are deduced from the static eigenvalues calculated from Eq. (45) and Eq. (46). Table 7 shows the corner functions which are added to a conventional wave function expansion for each of the four corners. The influence of the corner functions on the prediction results is shown in figure 9. This figure plots the predicted displacement in response point w_3 . The WB results are compared with an FE model of 348,564 degrees of freedom (element size $0.0056m$, λ_b at 175Hz $0.165m$). Both WB models contain wave functions of the first and second set ($T_1 = 1.5$). The prediction made by the WBM without corner functions (bottom figure) does not correspond well with the reference solution. Extending the set of wave functions with corner functions (top figure) improves the convergence of the WBM significantly and results in an accurate prediction.

Figure 10 compares the performance of the WBM and FEM. The figure gives the relative prediction error averaged over the $n_{rp} = 4$ response points, as a function of the computation time. Similar as for the U-shaped plate, the WBM with wave functions of both sets and corner functions gives the most accurate predictions. That is why only these WB models are included in the convergence analysis. The WB results are compared with a WB reference model, see table 8 for the model details. For the FEM, both models with a linear and

corner	angle	eigenfunction	eigenvalue
c	270°	$\Upsilon_{1,c} = \cos(\lambda_{1,c}\theta) \left(J_{\lambda_{1,c}}(k_b r) - C_{1,c} Y_{\lambda_{1,c}}(k_b r) - \frac{2}{\pi} C_{1,c} K_{\lambda_{1,c}}(k_b r) \right)$	$\lambda_{1,c} = 0.455516$
		$\Upsilon_{2,c} = \cos(\lambda_{1,c}\theta) \left(I_{\lambda_{1,c}}(k_b r) - C_{1,c} Y_{\lambda_{1,c}}(k_b r) - \frac{2}{\pi} C_{1,c} K_{\lambda_{1,c}}(k_b r) \right)$	
		$\Upsilon_{3,c} = \sin(\lambda_{1,c}^*\theta) \left(J_{\lambda_{1,c}^*}(k_b r) - C_{1,c}^* Y_{\lambda_{1,c}^*}(k_b r) - \frac{2}{\pi} C_{1,c}^* K_{\lambda_{1,c}^*}(k_b r) \right)$	$\lambda_{1,c}^* = 0.0914708$
		$\Upsilon_{4,c} = \sin(\lambda_{1,c}^*\theta) \left(I_{\lambda_{1,c}^*}(k_b r) - C_{1,c}^* Y_{\lambda_{1,c}^*}(k_b r) - \frac{2}{\pi} C_{1,c}^* K_{\lambda_{1,c}^*}(k_b r) \right)$	
		$\Upsilon_{5,c} = \cos(\lambda_{2,c}\theta) J_{\lambda_{2,c}}(k_b r)$	$\lambda_{2,c} = 1.54448$
		$\Upsilon_{6,c} = \cos(\lambda_{2,c}\theta) I_{\lambda_{2,c}}(k_b r)$	
		$\Upsilon_{7,c} = \sin(\lambda_{2,c}^*\theta) J_{\lambda_{2,c}^*}(k_b r)$	$\lambda_{2,c}^* = 1.90853$
		$\Upsilon_{8,c} = \sin(\lambda_{2,c}^*\theta) I_{\lambda_{2,c}^*}(k_b r)$	

Table 7: Eigenfunctions and eigenvalues for the hexagonal plate (c=7-10).

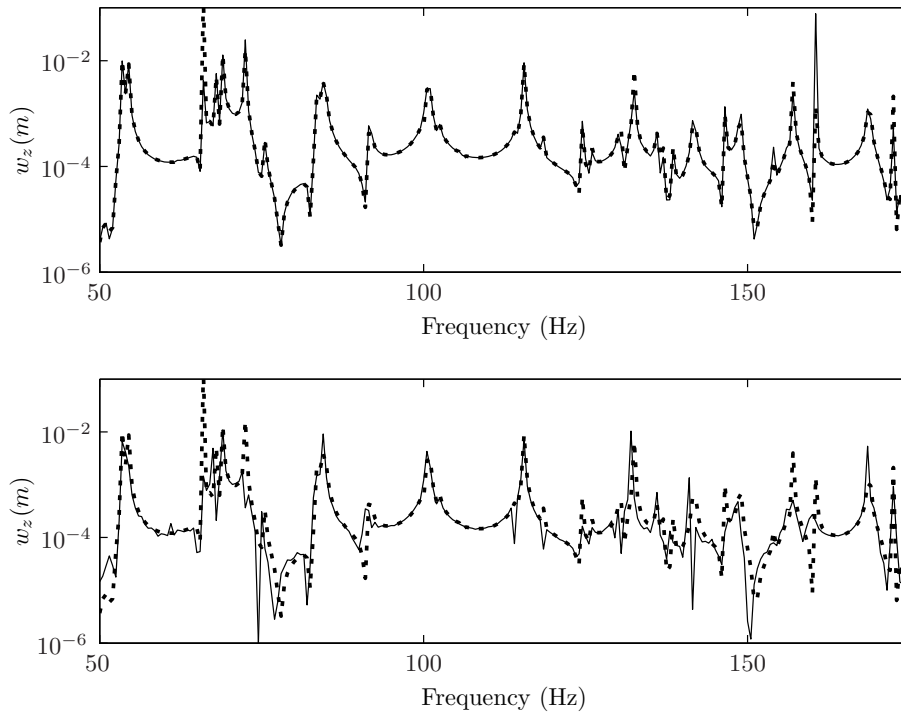


Figure 9: Frequency response function for response point w_3 (dashed: FE reference 348,564dofs / solid: WBM CF set1+2 (top), WBM set1+2 (bottom)).

frequency (Hz)	# WF set 1 domain 1+3	# WF set 2 domain 1+3	# WF set 1 domain 2+4	# WF set 2 domain 2+4	# CF
145	392	376	552	536	32
225	680	664	480	464	32
379	880	864	616	600	32

Table 8: WB reference models for the hexagonal plate.

frequency (Hz)	wavelength λ_b (m)	# FE dofs	element size (m)
145	0.181	2,685,480	0.0046
225	0.145	2,685,480	0.0046
379	0.112	2,685,480	0.0046

Table 9: FE reference models for the hexagonal plate.

quadratic discretisation are included. The FE results are compared with a quadratic FE reference model of 2,685,480 degrees of freedom, see table 9. Figure 10 indicates that also for this example the WBM has an enhanced convergence rate over both the linear and quadratic FEM.

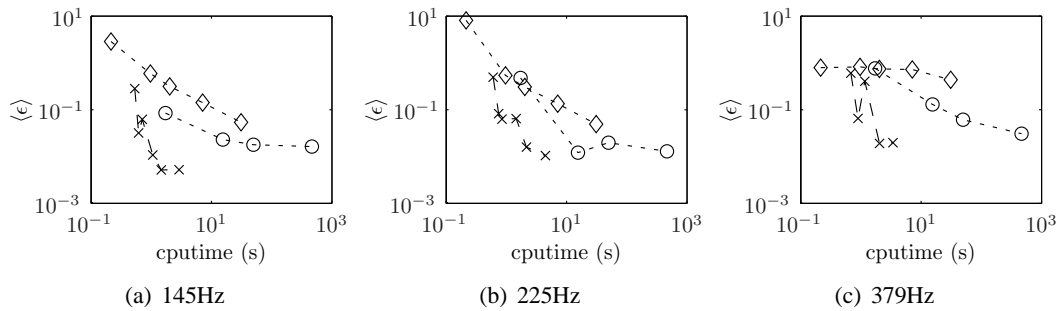


Figure 10: Convergence curves (— x — WBM CF set1+2 /— diamond — FEM linear /— circle — FEM quadratic).

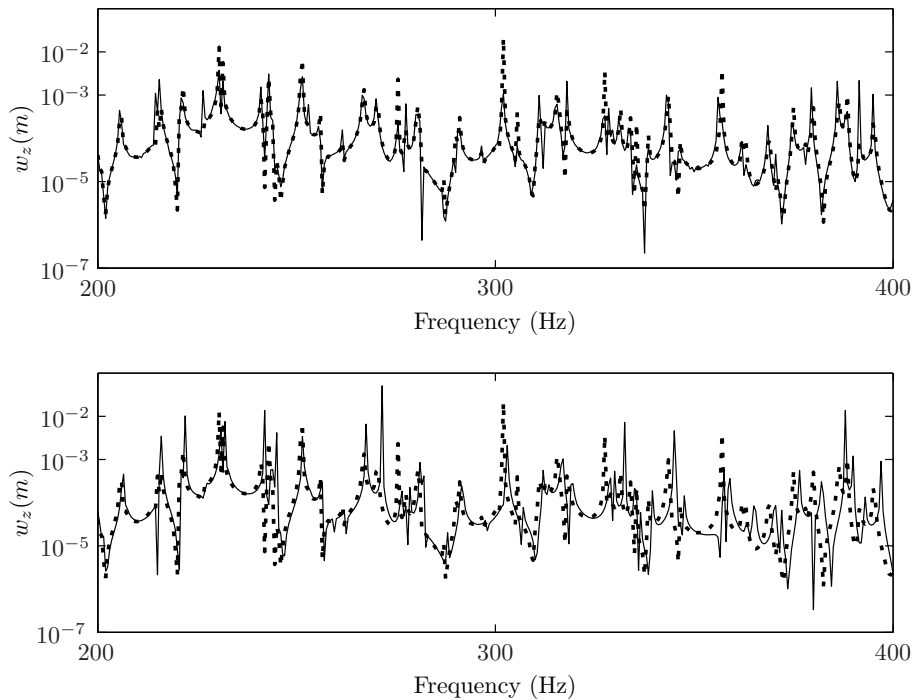


Figure 11: Frequency response function for response point w_3 (dashed: FE reference 348,564dofs / solid: WBM CF set1+2 (top), FEM 56,220dofs (bottom)).

Figure 11 plots the predicted displacement in response point w_3 in function of the frequency. The figure shows the prediction made by the WBM ($CF\ set1+2$) and the FEM. Both results are compared with a reference solution that was predicted with a linear FE model of 348,564 degrees of freedom (element size 0.0056m, λ_b at 400Hz 0.109m). The WB model is calculated with a truncation parameter $T_1 = 1.5$, leading to a model of 360 (set 1) plus 328 (set 2) wave functions at 200Hz and 496 (set 1) plus 464 (set 2) wave

functions at 400Hz. The number of corner functions is constant, i.e. 32. The WBM needs 1007 CPUseconds to calculate the entire response function from 10Hz to 400Hz. Figure 11 only shows the part of the response function between 200Hz and 400Hz, since below 200Hz both the FE and WB result correspond perfectly with the reference solution. As indicated by the top figure, the WB prediction corresponds very well with the reference solution over the entire frequency range. The FE model consists of 56,220 degrees of freedom (element size 0.014m) and needed 1493 CPUseconds to calculate the entire response function. At low frequencies, there is a good correspondence between the FE and reference solutions. But starting from 250Hz the FE results already suffer from dispersion errors such that some errors are induced in the prediction of the resonance frequencies. This confirms the enhanced convergence rate of the WBM, which enables the WBM to make accurate predictions up till higher frequencies than the FEM.

6 Conclusions and future research

The WBM is a novel numerical prediction technique with the potential to relax the frequency limitation of the element based prediction techniques, such as the FEM. This paper discusses the application of the WBM to plate bending with special focus on the treatment of stress singularities. Previous validations showed that the WBM suffers from convergence problems when singularities arise in the problem solution. For a polygonal plate domain, singularities can be expected in the plate corners if the interior angle exceeds a critical value, which depends on the type of boundary conditions along the edges adjacent to the corner. This paper proposes to extend the conventional set of wave functions with a number of corner functions that are capable of representing exactly the stress singularities. The corner functions are defined as the homogeneous solutions for an infinite wedge domain. However, it is only possible to define the exact solution if the two radial edges are both simply supported. For other combinations of radial boundary conditions, a procedure is presented to deduce the corner functions from Williams' static eigenfunctions. In this way the asymptotic behaviour around the corner is still identical to that of the exact solution. This results in an enhanced WBM that is capable of predicting accurate results, even when the solution becomes singular in one or more corners.

The potential of the enhanced WBM is demonstrated through two validation examples. In each example the solution exhibits stress singularities, which cause the conventional WBM to suffer from convergence problems. It was verified for the validation examples that extending the expansion of wave functions with a few corner functions for each corner where singularities occur, indeed resolves the convergence problems of the WBM. Furthermore, it was demonstrated that for non-convex problems the WBM that additionally includes wave functions of the second set shows to have an increased convergence rate. The performance of the WBM has also been compared with that of the FEM, where both a linear and quadratic discretisation are included. In all cases the WBM exhibits an increased convergence rate over the FEM. As a result, the WBM is capable of making accurate predictions up till higher frequencies than the FEM for a same computational load. This indicates the potential of the WBM as an efficient mid-frequency technique.

The main drawback of the WBM is its inability to deal with geometrically complex structures. Since for convergence purposes all subdomains have to be convex, a complex geometry requires a high number of subdomains which will drastically decrease the convergence rate of the method. Therefore a hybrid approach [16][17] is being envisaged. In this approach, the WBM will be coupled together with the FEM to combine the advantages of both methods. The WBM will be used to model the geometrically simple parts of the structures in a very efficient way. The FEM, on the other hand, will be used to model the geometrically more complex parts of the structure. This approach is especially appropriate for structures that exhibit a typical mid-frequency behaviour in the sense that some parts have already a short wavelength behaviour, while others still have a long wavelength behaviour. With the hybrid WB-FE approach, the WBM will be used to efficiently model the geometrically simple plate domains, that typically are still flexible in the mid-frequency range. The stiff components, on the other hand, will be modelled by the FEM.

Acknowledgements

The research work of Caroline Vanmaele is financed by a scholarship of the Institute for the Promotion of Innovation through Science and Technology in Flanders (IWT-Vlaanderen).

References

- [1] O.C. Zienkiewicz, R.L. Taylor, J.Z. Zhu, P. Nithiarasu, *The Finite Element Method - Vol. 1: Basic formulation and linear problems*, Butterworth-Heinemann (2005).
- [2] R.H. Lyon, R.G. DeJong, *Theory and application of statistical energy analysis - second edition*, Butterworth-Heinemann, Boston et al. (1995).
- [3] E. Trefftz, *Ein Gegenstück zum Ritschen Verfahren*, in *Proceedings of the 2nd International Congress on Applied Mechanics, Zürich, Switzerland*, Zürich (1926), pp. 131-137.
- [4] J. Robinson, *An evaluation of skew sensitivity of thirty three plate bending elements in nineteen FEM systems*, Finite Element News - special report (1985).
- [5] R.H. MacNeal, *Finite Elements: their design and performance*, Marcel Dekker Inc, New York (1994).
- [6] C. Vanmaele, W. Desmet, D. Vandepitte, *A wave based prediction technique for the steady-state dynamic analysis of flat plate assemblies*, in *Proceedings of the European Congress on Computational Methods in Applied Sciences and Engineering, Eccomas 2004, Jyväskylä, Finland, Jyväskylä* (2004).
- [7] C. Vanmaele, D. Vandepitte, W. Desmet, *An efficient Wave Based prediction technique for plate bending vibrations*, Computer methods in applied mechanics and engineering, submitted for publication.
- [8] J. Jirousek, L. Guex, *The hybrid-Trefftz finite element model and its application to plate bending*, International Journal of Numerical Methods in Engineering, Vol. 23 (1986), pp. 651-693.
- [9] A. Leissa, O.G. McGee, C.S. Huang, *Vibrations of Sectorial Plates having Corner Stress Singularities*, Journal of Applied Mechanics, Vol. 60 (1993), pp. 134-140.
- [10] A. Leissa, *Vibration of plates*, Acoustical Society of America, Woodbury, New York (1993).
- [11] M. Abramowitz, I.A. Stegun, *Handbook of Mathematical Functions*, Dover Publications, New York (1970).
- [12] M.L. Williams, *Surface Stress Singularities Resulting from various Boundary Conditions in Angular Plates under Bending*, in *Proceedings of the First U.S. National Congress of Applied Mechanics* (1952), pp. 325-329.
- [13] A.W. Leissa, O.G. McGee, C.S. Huang, *Vibrations of Circular Plates having V-Notches or sharp radial cracks*, Journal of Sound and Vibration, Vol. 161 (1993), pp. 227-239.
- [14] W. Desmet, *A Wave based prediction technique for coupled vibro-acoustic analysis*, Ph.D. dissertation, Katholieke Universiteit Leuven, Departement Werktuigkunde, Leuven (1998).
- [15] M. J. D. Powell, *A Fortran Subroutine for Solving Systems of Nonlinear Algebraic Equations*, in P. Rabinowitz editor, *Numerical Methods for Nonlinear Algebraic Equations, Ch.7* (1970).
- [16] B. Van Hal, W. Desmet, D. Vandepitte and P. Sas, *Coupled finite element - wave based approach for the steady-state dynamic analysis of acoustic systems*, Journal of Computational Acoustics, Vol. 11, No. 2 (2003).

- [17] C. Vanmaele, W. Desmet, D. Vandepitte, *A direct hybrid Finite Element - Wave Based prediction technique for the steady-state dynamic analysis of two-dimensional solids*, in *proceedings of ICSV12, Lisbon, Portugal, Lisbon (2005)*.